




# Metacomposites: functional design via titanium nitride/nickel(II) oxide composites towards tailorable negative dielectric properties at radio-frequency range

Yunpeng Qu<sup>1,2</sup> · Yuyan Li<sup>4</sup> · Ciqun Xu<sup>1,2</sup> · Guohua Fan<sup>1,2</sup> · Peitao Xie<sup>1,2</sup> · Zhongyang Wang<sup>1,2</sup> · Yao Liu<sup>1</sup>  · Yulin Wu<sup>1</sup> · Runhua Fan<sup>3</sup>

Received: 27 November 2017 / Accepted: 6 January 2018 / Published online: 13 January 2018  
© Springer Science+Business Media, LLC, part of Springer Nature 2018

## Abstract

Functional metacomposites towards negative dielectric properties via percolating behavior have triggered tremendous fundamental and practical interest. In this paper, titanium nitride was selected to construct percolating metacomposites. Hence, adjusting the frequency region and the value of negative permittivity was effectively realized by uniformly building different ratio  $x$  of nickel(II) oxide/titanium nitride composites. Occurrence of percolation phenomenon and change of conductive mechanism were observed when alternating the ratio  $x$ . Two different types of negative permittivity (i.e., dipole-type and plasma-type) were observed in the composites. The dipole-type negative permittivity behavior in the composite with low titanium nitride content (i.e.,  $x=0.5$ ) was ascribed to the resonance-induced electric dipole generated from the isolated titanium nitride particles, which could be explained by Lorentz model. While the plasma-type negative permittivity with titanium nitride content exceeding the percolation threshold could be well explained by the low frequency plasmonic state generated from conductive titanium nitride networks using Drude model. Besides, the electrical properties influenced by percolating phenomenon including ac conductivity, dielectric loss, and impedance were investigated. This work presents a systematic and novel investigation on negative dielectric properties of percolating metacomposites and will greatly facilitate the practical applications of metacomposites.

**Electronic supplementary material** The online version of this article (<https://doi.org/10.1007/s10854-018-8557-7>) contains supplementary material, which is available to authorized users.

✉ Yao Liu  
liuyao@sdu.edu.cn

- <sup>1</sup> Key Laboratory for Liquid-Solid Structural Evolution and Processing of Materials (Ministry of Education), Shandong University, Jinan 250061, China
- <sup>2</sup> Dezhou META Research Center for Innovative Materials, Dezhou 253000, China
- <sup>3</sup> College of Ocean Science and Engineering, Shanghai Maritime University, Shanghai 201306, China
- <sup>4</sup> School of Chemical Engineering and Technology, China University of Mining and Technology, Xuzhou 221000, China

## 1 Introduction

The percolating phenomenon, a classic and significant behavior in physics widespreading in heterogeneous multi-components of materials [1–4], has drawn intensive attention due to their fascinating properties and potential applications in the field of thermal storage [5], light-emitting diodes [6], and charge-storage capacitors [7], etc. Specifically, once the concentration of functional fillers in the percolating composites approaches a critical value (i.e., percolation threshold), the filler particles come into contact with each other and establish a continuous network throughout the system [8–10]. Along with the change of microstructure, the physical properties of the composites also undergo an abrupt shift and bring about attractive performances, such as high dielectric constant or high electrical or thermal conductivity [11, 12].

Interestingly, several studies recently found that negative electromagnetic parameters (i.e. permittivity  $\epsilon'$  and permeability  $\mu'$ ) can be achieved when functional fillers exceeded the percolation threshold which could combine

with metacomposites constructing [13, 14]. Metacomposites designation towards negative permittivity via percolating behavior was distinguished from traditional metamaterials built by many artificially periodic unit cells. And percolating metacomposites performed preferable experimental reproducibility, great feasible regulation and environment-friendly properties [4, 8, 15–17] which effectively broadened the applying fields of metamaterials. Therein, metallic fillers (i.e. Fe, Co, Ni) [18–23] and carbonaceous materials [24–27] were used to prepare metacomposites, while few attentions was put on conductive ceramic fillers. Especially, titanium nitride (TiN), which possessed great chemical stability, temperature durability and impedance match, exhibited a plasmonic resonance in visible–NIR range [28–30].

Thus, we combined titanium nitride and nickel(II) oxide (NiO) to construct metacomposites towards negative dielectric properties, while their electrical performances influenced by percolating behavior including negative permittivity, ac conductivity, dielectric loss and impedance properties were systematically investigated at radio-frequency range. More concretely, the frequency region and value of negative permittivity are effectively adjusted by homogenizing different ratio  $x$  of TiN and NiO. Percolation phenomenon and conductive mechanism changes were observed when alternate the ratio  $x$ . Two different types of negative permittivity (i.e., dipole-type and plasma-type) were observed in the composites. The dipole-type negative permittivity behavior in the composite with low titanium nitride content (i.e.,  $x=0.5$ ) was ascribed to the resonance-induced electric dipole generated from the isolated titanium nitride particles, which could be explained by Lorentz model. While the plasma-type negative permittivity with titanium nitride content exceeding the percolation threshold could be well explained by the low frequency plasmonic state generated from conductive titanium nitride networks using Drude model. As for nickel(II) oxide, it severed as capacitor materials to form many micro capacitors by uniformly distributing among titanium nitride particles, and was selected because of its satisfactory electric insulation, chemical inertness and temperature durability and other similar physical properties as titanium nitride [31, 32].

## 2 Materials and methods

Titanium nitride (purity 99.5%, average size  $\sim 6 \mu\text{m}$ ) and nickel(II) oxide (purity 98%, average size  $\sim 2 \mu\text{m}$ ) were purchased from Sinopharm Chemical Reagent Co. Ltd. The composites with titanium nitride contents of 0, 40, 45, 50, 60, 70, 75, 80, 85, 90, 100 wt% were prepared by blending and compression molding procedure followed by annealing in nitrogen at 873 K to enhance their solidity and strength. The microstructure of composites was investigated by SU-70

field emission scanning electron microscopy (FESEM). The phase composition of all samples was measured by an X-ray diffractometer (XRD, XD2/3, Beijing Purkinje General Instrument Co., Ltd, Beijing, China) with Cu  $K_{\alpha}$  radiation in air at room temperature. The dielectric properties of composites at radio frequency was tested by Agilent E4991A precision impedance analyzer. For permittivity measurement, all samples were processed into cylinders (20 mm  $\times$  20 mm  $\times$  2 mm). Before the test, the open/short compensation and load compensation was performed to reduce the residual impedances of the test fixtures and calibrate the test fixtures [33]. Permittivity was measured via putting samples between the two planar electrodes of the 16453A dielectric test fixture. The output data was impedance ( $Z'$ ,  $Z''$ ), capacitance ( $C_p$ ) and resistance ( $R_p$ ) which could be used for calculation of impedance modulus value ( $|Z|$ ), complex permittivity ( $\epsilon'$ ,  $\epsilon''$ ) and ac conductivity ( $\sigma_{ac}$ ).

Specifically and respectively:

$$\epsilon' = \frac{hC_p}{S\epsilon_0} \quad (1)$$

$$\epsilon'' = \frac{h}{2\pi fSR_p\epsilon_0} \quad (2)$$

$$\sigma_{ac} = \frac{h}{R_pA} \quad (3)$$

$$|Z| = \sqrt{|Z'|^2 + |Z''|^2} \quad (4)$$

$$\tan \delta = \frac{\epsilon''}{|\epsilon'|} \quad (5)$$

where  $h$  is the thickness of the sample,  $S$  is the area of the electrode,  $\epsilon_0$  is the absolute permittivity of free space ( $8.85 \times 10^{-12}$  F/m),  $f$  is the frequency of the electric field,  $A$  is the area of the contact medium, and  $\tan \delta$  is dielectric loss tangent.

## 3 Results and discussion

### 3.1 Microstructure characterization

The ideal model of three-dimensional conductive networks formed in TiN/NiO composites were schematic in Fig. 1 based on the SEM images (shown in Figs. S1 and S2). This three-dimensional networks, key to percolating behavior which brings huge variation of properties (i.e. permittivity), should be investigated and discussed (shown in “[Negative permittivity behavior](#)” section in detail). Besides, the

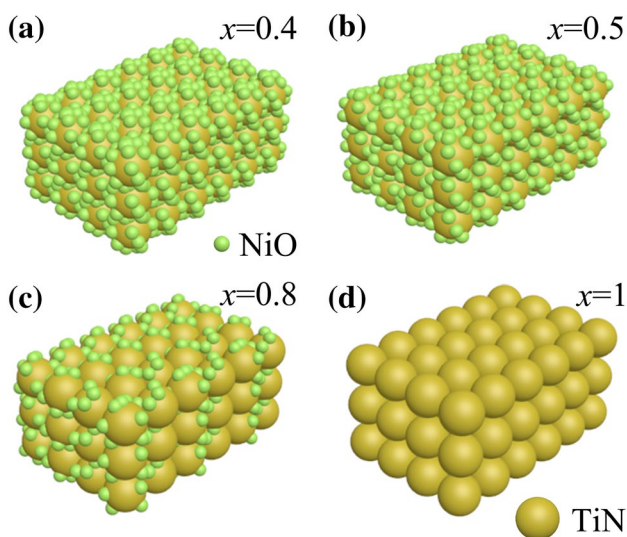


Fig. 1 Schematic diagram of ideal microstructure in TiN/NiO meta-composites according to the real SEM images shown in supplying information

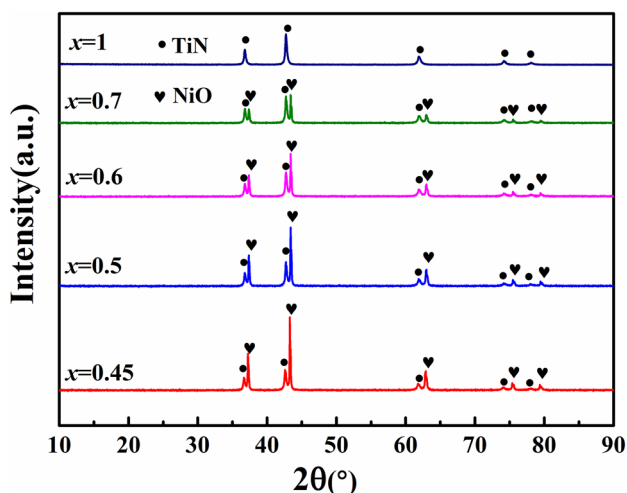


Fig. 2 XRD patterns of TiN and TiN/NiO composites with different TiN contents

characteristic peaks of TiN and NiO are clearly observed in Fig. 2, while the intensity of TiN peaks is increasing with increasing  $x$ .

### 3.2 Conductivity behavior

Figure 3 shows the frequency dependent ac conductivity ( $\sigma_{ac}$ ) for the TiN and its composites with different ratio  $x$  of TiN/NiO. The  $\sigma_{ac}$  increases on increasing the frequency of the composites with a content of not more than  $x=0.5$  (50 wt%), while the  $\sigma_{ac}$  decreases as the frequency increases for composites with higher TiN content. The different

variation trends of  $\sigma_{ac}$  depending on the frequency indicate different conductive mechanisms, and a percolation phenomenon occurs in the composites on increasing the TiN content. The percolation threshold is between  $x=0.5$  and  $x=0.6$  which is verified by the different conductive model. For composites below the percolation threshold, the  $\sigma_{ac}$ - $f$  relationship obeys the formula [18]:

$$\sigma_{ac} = \sigma_{dc} + A(2\pi f)^n \tag{6}$$

where  $\sigma_{dc}$  is direct current conductivity,  $f$  is the frequency,  $A$  is the pre-exponential factor and  $n$  is the fractional exponent ( $0 < n < 1$ ). As shown in Fig. 3b, dc conductance was primary at low frequency while ac conductance gradually dominated as increasing  $f$  to high frequency region. This is suggestive of a hopping conduction behavior in the composites which means free electrons can “jump” between adjacent TiN particles under the action of an external electric field [34]. When the TiN content exceeds the percolation threshold, the TiN particles are connected to each other to form a three-dimension conducting network throughout the composites, which results in a metal-like conductive behavior, e.g. at low frequencies,  $\sigma_{ac}$  was almost independent of frequency; at high frequencies,  $\sigma_{ac}$  decreases with increasing frequency which should be attributed to the skin effect (when an alternating electric current flows through a conductor, the electric mainly flows at the “skin” of the conductor, which is called the skin effect) [8].

The skin depth can be expressed as [35]:

$$\delta = \left( \frac{2}{\omega \mu \sigma_{dc}} \right)^{\frac{1}{2}} \tag{7}$$

where  $\delta$  is the skin depth,  $\omega$  is the angular frequency,  $\sigma_{dc}$  is the dc conductivity, and  $\mu$  is the static permeability of the composites. The increasing frequency will reduce the skin depth and enhance the skin effects [18]. Hence, the  $\sigma_{ac}$  of composites decreases with increasing the frequency, especially at high frequencies.

And the frequency dependence of  $\sigma_{ac}$  with  $x > 0.5$  follows the Drude model [35]:

$$\sigma_{ac} = \frac{\sigma_{dc} \omega_{\tau}^2}{\omega^2 + \omega_{\tau}^2} \tag{8}$$

$$\sigma_{dc} = \frac{Ne^2 \tau}{m} = \frac{\omega_p^2 \tau}{4\pi} \tag{9}$$

where  $\sigma_{dc}$  is the dc limit of the conductivity,  $\omega_{\tau}$  ( $\omega_{\tau} = 1/\tau$ ) is the relaxation rate and denotes the broadening of the oscillator due to damping, and  $\omega_p$  describes the oscillator strength, and is referred to the plasma frequency.

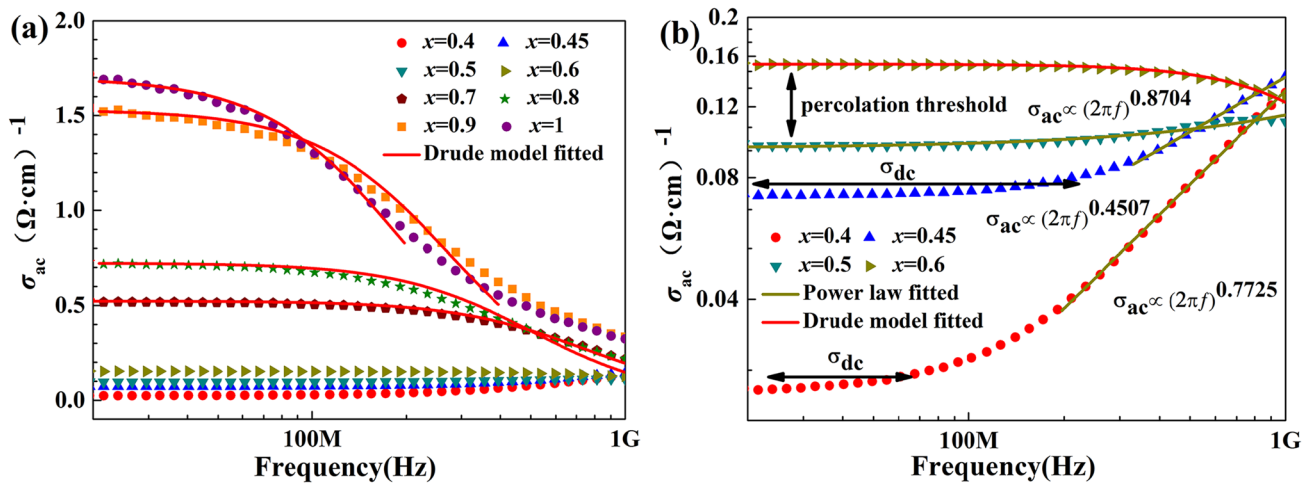


**Fig. 3** Frequency dependences of ac conductivity for the TiN and TiN/NiO composites with different TiN content **(a, b)**, the red and dark yellow solid lines in **(a, b)** are fitting results using Drude model and Jonscher’s power law, respectively. (Color figure online)

### 3.3 Negative permittivity behavior

Frequency dispersions of the real permittivity ( $\epsilon'$ ) with different TiN contents are given in Fig. 4a, b. For  $x = 0.4$  and  $0.45$ , it was found that the values of  $\epsilon'$  were positive and enhanced with increasing TiN content over the whole frequency, which could be ascribed to increasing micro-capacitors formed by isolated TiN and NiO particles in the composites [36]. In addition, interfacial polarization (Maxwell–Wagner–Sillars effect) also gave rise to the improvement of permittivity [37, 38]. Especially, for the curves from TiN/NiO ( $x = 0.4, 0.45, 0.5$ ) composites (below the percolation threshold) showed in Fig. 4b, it was observed that the  $\epsilon'$  decreased with gradually increasing frequency and huge decreasing variations happened at high frequency range. Hence, the real permittivity ( $\epsilon'$ ) of TiN/NiO ( $x = 0.5$ ) composite (quite closing to percolation threshold) turned from positive to negative when increasing frequency reached about 690 MHz which could be ascribed to Lorentz resonance:[15, 39, 40].

$$\epsilon^* = \epsilon' - i\epsilon'' = 1 + \frac{\omega_p^2}{\omega_0^2 + \omega^2 + i\Gamma_L\omega} \tag{10}$$

$$\epsilon' = 1 + \frac{\omega_p^2(\omega_0^2 - \omega^2)}{(\omega_0^2 - \omega^2)^2 + \omega^2\Gamma_L^2} \tag{11}$$

where  $\omega$  ( $\omega = 2\pi f$ ) is the angular frequency of the electric field,  $\omega_0$  ( $\omega_0 = 2\pi f_0$ ) is the characteristic frequency (or resonance frequency),  $\omega_p$  ( $\omega_p = 2\pi f_p$ ) is the angular plasma frequency describing the resonance strength, and  $\Gamma_L$  represents the damping constant related to the broadening of resonance.

The Lorentz type dielectric resonance should result from the induced electric dipole in the isolated TiN particles [8]. When the frequency of the external electric field reaches the resonance frequency range (near  $f_0$ ), negative permittivity may be obtained [8]. Such type negative permittivity behavior were also observed in composites that carbon nanotubes (CNTs) or graphene served as functional fillers [14, 15].

The negative permittivity also appeared when the TiN content exceeded percolation threshold, which was attributed to the formation of the three-dimension interconnected TiN networks [20] in the composites illustrated by Fig. 1. As shown in Fig. 4a, the  $\epsilon'$  of the composites with the higher TiN contents ( $x > 0.5$ ) kept negative over the whole frequency. Theoretically, the plasma-type negative permittivity behavior can be described by Drude model, which gives a frequency dependence of the permittivity for delocalized electrons [18]. As shown in Fig. 4a, the relationship of negative  $\epsilon'$  versus frequency agrees well with the results fitted by Drude model [18]:

$$\epsilon^* = \epsilon' - i\epsilon'' = 1 - \frac{\omega_p^2}{\omega^2 + i\omega\Gamma_D} \tag{12}$$

$$\epsilon' = 1 - \frac{\omega_p^2}{\omega^2 + \Gamma_D^2} \tag{13}$$

$$\omega_p = \sqrt{\frac{n_{eff}e^2}{m_{eff}\epsilon_0}} \tag{14}$$

where  $\Gamma_D$  is the damping constant,  $\omega_p = 2\pi f_p$  is plasmons angular frequency,  $n_{eff}$  is effective concentration of electron,

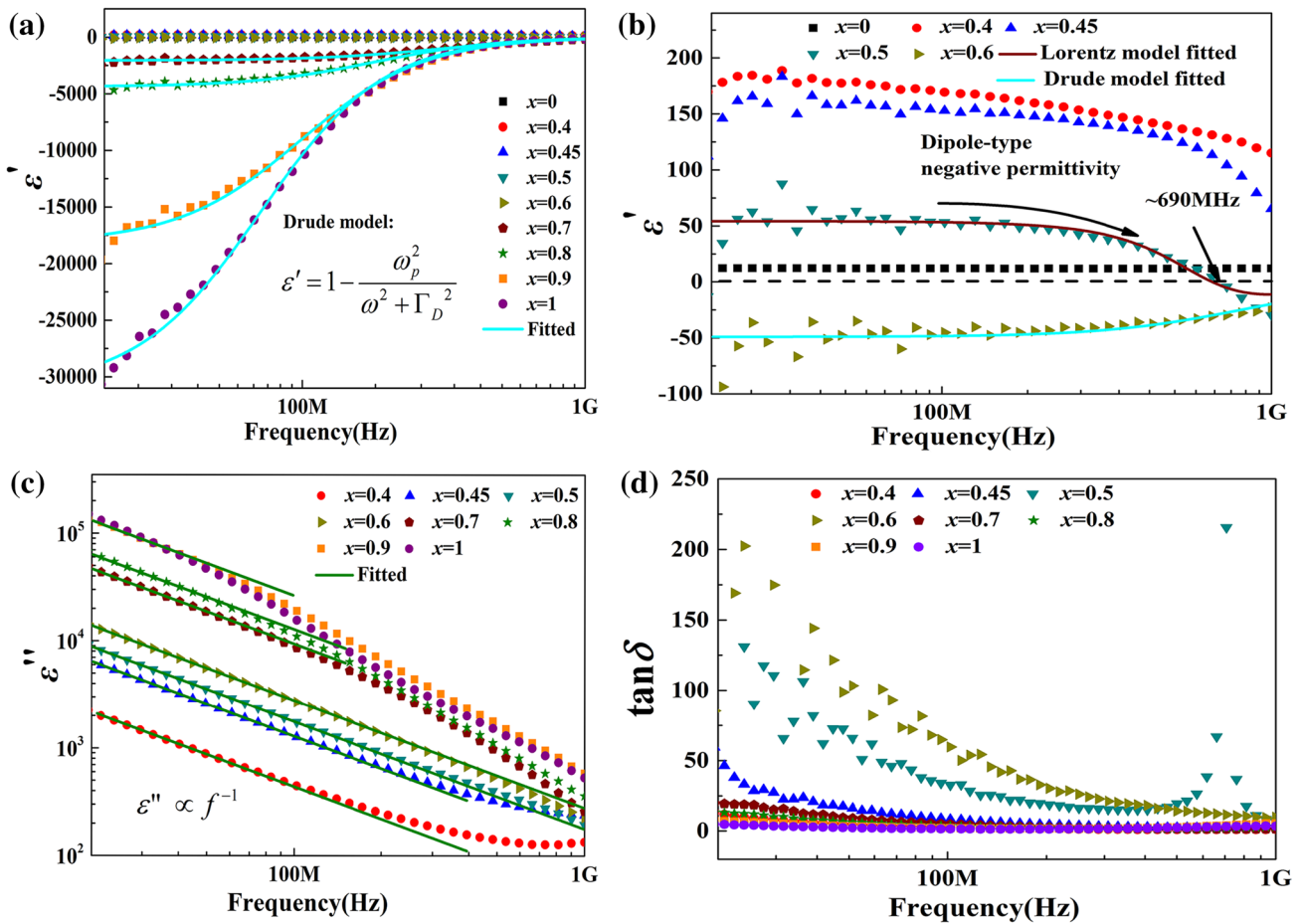


**Fig. 4** Frequency dependences of real permittivity ( $\epsilon'$ ) for TiN and TiN/NiO composites (a, b), the cyan and wine solid lines in (a, b) are fitting results using Drude model and Lorentz model, respectively.

Frequency dependences of the imaginary permittivity ( $\epsilon''$ ) (c) and dielectric loss tangent ( $\tan\delta$ ) (d) for TiN and TiN/NiO composites. (Color figure online)

$m_{\text{eff}}$  is effective weight of electron, and  $\epsilon_0$  is vacuum permittivity ( $8.85 \times 10^{-12}$  F/m).

The imaginary permittivity ( $\epsilon''$ ) is known to be useful to evaluate the dielectric loss of materials [41]. In the case of the percolative composite system, the dielectric loss, which is closely associated with the frequency and concentration of conductive fillers, mainly originates from the conduction process, surface polarization and dipole movement [41, 42]. Thus  $\epsilon''$  can be expressed by Eq. (15) [8]:

$$\epsilon'' = \epsilon''_C + \epsilon''_D + \epsilon''_P \tag{15}$$

where  $\epsilon''_C$  is conduction loss,  $\epsilon''_D$  is dipolar loss and  $\epsilon''_P$  is interfacial polarization related loss. Generally, the interfacial polarization phenomenon occurs at low frequency, which is no more than 1 MHz [3]. Once the frequency of the external electric field reaches a high enough level, the charges do not have time to accumulate at the interface, leading to the disappearance of interfacial polarization. Therefore, the dielectric loss mainly includes the conduction loss and dipolar loss

in our test frequency (20 MHz–1 GHz). The conduction loss arises from a leakage current among conductive fillers or the contact resistors in the circuit model, and can be described by [42]:

$$\epsilon''_C = \frac{\sigma_{dc}}{2\pi f \epsilon_0} \tag{16}$$

The  $\sigma_{dc}$  is constant for a given material, so the  $\epsilon''_C$  is inversely related to  $f$  ( $\epsilon''_C \propto f^{-1}$ ). The dipolar loss stems from polarization currents and the movement of dipoles on continuously changing the electric fields [41].

Figure 4c presents the  $\epsilon''$  versus frequency for the TiN and its composites with different ratio  $x$ . The incorporation of TiN particles leads to an evident increment of  $\epsilon''$ . For the composites under the percolation threshold, the plots of  $\epsilon''$  versus  $f$  exhibit the liner decrease relationship in the low frequency, and then demonstrate a nonlinear increasing trend at the high frequency region. That is, there is a change of the dominant role in the dielectric loss from the conduction loss to the

dipolar loss on increasing the frequency [8]. The results can be understood by the reason that the conductivity loss decreases with increasing the frequency [according to Eq. (16)], and the contribution from the dipolar loss becomes more significant at high frequency.

Figure 4d corresponds to the frequency dependence of  $\tan\delta$ . It was found that  $\tan\delta$  was larger when ratio  $x$  was closer to the percolation threshold (shown in Fig. S4). Specially, there was a peak at about 690 MHz for TiN/NiO composites ( $x=0.5$ ), which could be explained by the Eq. (5). When  $\epsilon'$  shifts from positive to negative at about 690 MHz, there must be an increasing and decreasing trend (which means peak) near this shift frequency.

### 3.4 Impedance and equivalent circuit analysis

The relationship for different circuit elements can be expressed as [43]:

$$Z = \frac{\dot{U}}{I} = R + j(X_L - X_C) = Z' + jZ'' \quad (17)$$

$$\varphi = \arctan \frac{X}{R} = \arctan \frac{X_L - X_C}{R} \quad (18)$$

To further explore the negative dielectric properties of the composites, equivalent circuit analysis using Zsimpwin software was performed to investigate the impedance spectra of composites shown in Fig. 5. For the positive permittivity composites ( $x=0.4$  and  $0.45$ ), the reactance showed negative values in the whole frequency regime (Fig. 5a). As illustrated in Fig. 6a, when  $X_L < X_C$ , then  $U_L < U_C$ , thus  $\varphi < 0$

which means that the phase of voltage lags behind the phase of current, indicating a capacitive character. Their equivalent circuits consist of a series resistor ( $R_1$ ) with a parallel connection of a resistor ( $R_2$ ) and a capacitor ( $C_p$ ) (inset of Fig. 5a). The  $R_1$  came from the silver electrode with a small value [44]. The  $R_2$  resulted from the leakage current of composites, and decreased with increasing ratio  $x$ , indicating better conductivity [45]. The  $C_p$  was mainly derived from the microcapacitors formed by the TiN and NiO particles in the composites [46]. The isolated TiN particles usually

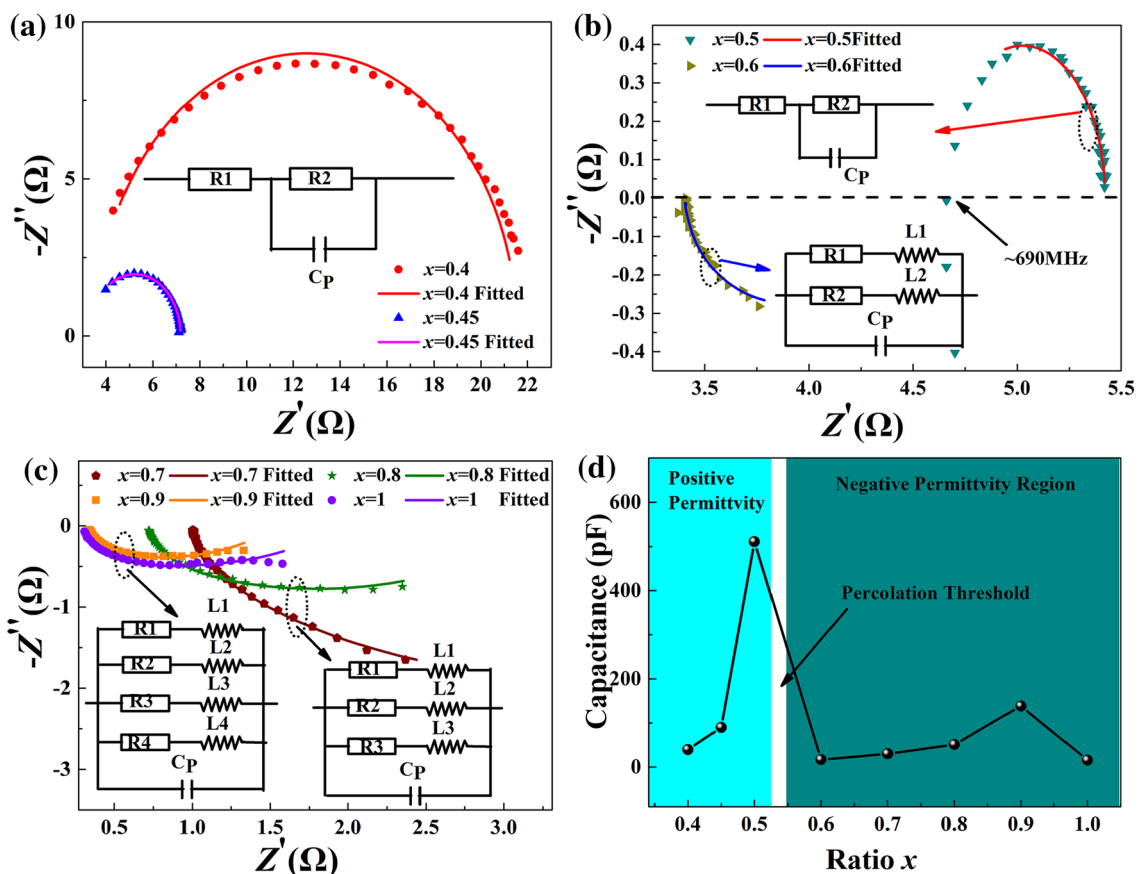


**Fig. 5** Nyquist plot (a–c) for the TiN and TiN/NiO composites. The solid lines in (a–c) are fitting results using equivalent circuit. The variation of capacitance from equivalent circuit elements with differ-

ent ratio  $x$  (d), the other corresponding parameters of the simulating results were presented in Table S3 in Supporting Information. (Color figure online)

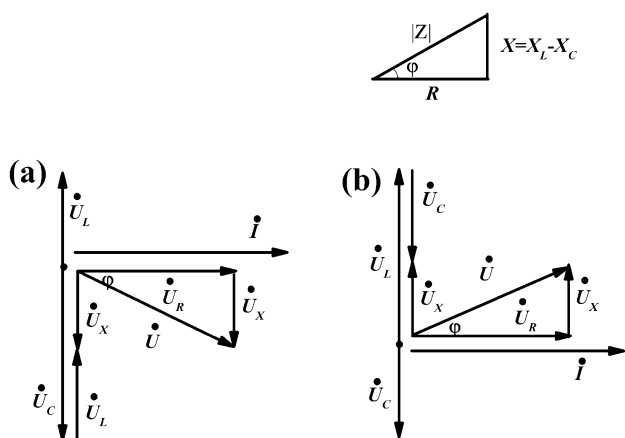


**Fig. 6** Phasor diagram of voltage versus current and relationship with complex impedance in a series connected *RLC* circuit.  $\dot{U}$ ,  $\dot{I}$ ,  $\dot{U}_R$ ,  $\dot{U}_L$ ,  $\dot{U}_X$  and  $\dot{U}_C$  are voltage or current phasor for different circuit elements,  $\varphi$  is the impedance angle,  $X_L$ ,  $X_C$  and  $X$  are reactance

manifested capacitive character until network formed, however, there is an exception for composite ( $x=0.5$ ) near percolation threshold, shown in Fig. 5b. It presents capacitive character with negative reactance at low frequency, while further increasing frequency, the reactance changed from negative to positive at nearly 690 MHz corresponding to the positive–negative permittivity switching point. That is to say,  $\varphi < 0$  was changed to  $\varphi > 0$ , the composites change from capacitive to inductive and the conductive mechanism changes from hopping conduction to metal-like conduction.

The reactance was positive in the overall test frequency range for samples ( $x=0.6, 0.7, 0.8, 0.9, 1$ ), which means  $X_L > X_C$ , then  $U > U$  and  $\varphi > 0$  [derived from Eqs. (17) and (18)], manifesting the inductive character. Inductors were introduced into their equivalent circuit due to the formation of conductive TiN network (inset of Fig. 5b, c). Inductor is a spatial conductive loop with a spiral shape, and the relationship between  $L(\mu H)$  and geometric dimensions can be expressed as [17]:

$$L = \frac{\mu_0 N^2 \pi D^2}{l} \tag{19}$$

where  $D$  (cm) is the loop diameter,  $N$  is the winding number, and  $l$  is the loop length (cm).  $l$  is a constant, i.e., the sample thickness. There was two inductor for the composites of  $x=0.6$ , and three inductors of  $x=0.7$  and  $0.8$ , four inductors of  $x=0.9$  and  $1$  which could be explained by new conductive paths formed as increasing the ratio  $x$  (shown in Fig. 7), leading to the increase of inductor number.

The appearance of circuit elements (i.e. inductors) has demonstrated the negative permittivity qualitatively, thus the capacitance should also be considered in order to further

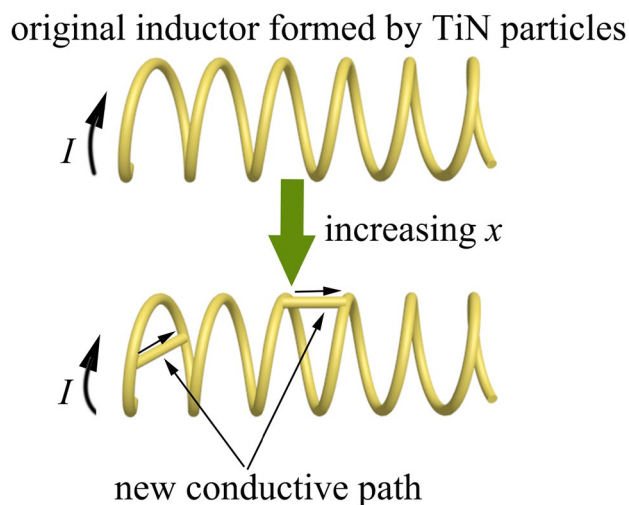


**Fig. 7** Schematic diagram of the structural variation of the inductor

investigate the relationship between percolation behavior and negative permittivity. Figure 5d shows the variation of capacitance from equivalent circuit elements with ratio  $x$ . There was also a percolation behavior corresponding to the positive–negative permittivity percolation. Below the percolation threshold, the capacitance increases with increasing ratio  $x$  in the positive permittivity region (in Fig. 5d), explained by Maxwell–Wagner–Sillars effect. At the percolation region, the capacitance suddenly reduces due to the formation of the conductive network. With the assistance of the above analysis, a corresponding relationship between negative dielectric properties and percolating phenomenon was built and confirmed which could present fundamental reference resources for further researching and application in negative permittivity metamaterials.

### 4 Conclusion

In conclusion, percolating metamaterials in titanium nitride/nickel(II) oxide composites towards negative dielectric properties were constructed. The frequency region and the value of negative permittivity was effectively adjusted with different ratio  $x$ . Percolation phenomenon and conductive mechanism changes were observed when alternate the ratio  $x$ . The dipole-type negative permittivity behavior in the composite with low titanium nitride content (i.e.,  $x=0.5$ ) was ascribed to the resonance-induced electric dipole generated from the isolated titanium nitride particles, which could be explained by Lorentz model. While the plasma-type negative permittivity with titanium nitride content exceeding the percolation threshold could be well explained by the low frequency plasmonic state generated from conductive titanium nitride networks using Drude model. Moreover, negative

dielectric properties were investigated via equivalent circuit analysis to conclude a corresponding relationship between negative dielectric properties and percolating phenomenon which will surely facilitate the designation and application of metamaterials.

**Acknowledgements** This study was financially supported by the National Natural Science Foundation of China [Grant Nos. 51771104 and 51402170].

## References

- C.W. Nan, Physics of inhomogeneous inorganic materials. *Prog. Mater. Sci.* **37**, 1–116 (1993)
- D.J. Bergman, D. Stroud, Physical properties of macroscopically inhomogeneous media. *Solid State Phys.* **46**, 147–269 (1992)
- C.W. Nan, Y. Shen, J. Ma, Physical properties of composites near percolation. *Annu. Rev. Mater. Res.* **40**, 131–151 (2010)
- K. Sun, R. Fan, Y. Yin, J. Guo, X.F. Li, Y. Lei, L. An, C. Cheng, Z. Guo, Tunable negative permittivity with fano-like resonance and magnetic property in percolative silver/yttrium iron garnet nanocomposites. *J. Phys. Chem. C* **121**, 7564–7571 (2017)
- R. Zheng, J. Gao, J. Wang, S.P. Feng, H. Ohtani, J. Wang, G. Chen, Thermal percolation in stable graphite suspensions. *Nano Letters* **12**, 188–192 (2012)
- M.S. White, M. Kaltenbrunner, E.D. Glowacki, K. Gutnichenko, G. Kettlgruber, I. Graz, S. Aazou, C. Ulbricht, D.A.M. Egbe, M.C. Miron, Ultrathin, highly flexible and stretchable PLEDs. *Nat. Photonics* **7**, 811–816 (2013)
- Z. Shi, J. Wang, F. Mao, C. Yang, C. Zhang, R. Fan, Significantly improved dielectric performances of sandwich-structured polymer composites induced by alternating positive-k and negative-k layers. *J. Mater. Chem. A* **5**, 14575–14582 (2017)
- C. Cheng, R. Fan, Y. Ren, T. Ding, L. Qian, J. Guo, X. Li, L. An, Y. Lei, Y. Yin, Radio frequency negative permittivity in random carbon nanotubes/alumina nanocomposites. *Nanoscale* **9**, 5779–5787 (2017)
- Z. Zhang, R. Fan, Z. Shi, S. Pan, K. Yan, K. Sun, J. Zhang, X. Liu, X.L. Wang, S.X. Dou, Tunable negative permittivity behavior and conductor–insulator transition in dual composites prepared by selective reduction reaction. *J. Mater. Chem. C* **1**, 79–85 (2013)
- Z. Shi, S. Chen, R. Fan, X. Wang, X. Wang, Z. Zhang, K. Sun, Ultra low percolation threshold and significantly enhanced permittivity in porous metal–ceramic composites. *J. Mater. Chem. C* **2**, 6752–6757 (2014)
- Y. Su, Y. Gu, S. Feng, Composites of NBCTO/MWCNTs/PVDF with high dielectric permittivity and low dielectric loss. *J. Mater. Sci. Mater. Electron.* (2017). <https://doi.org/10.1007/s10854-017-8160-3>
- W. Yang, H. Li, J. Lin, G. Chen, Y. Wang, L. Wang, H. Lu, L. Chen, Q. Lei, A novel all-organic DIPAB/PVDF composite film with high dielectric permittivity. *J. Mater. Sci. Mater. Electron.* **28**, 1–9 (2017)
- G. Fan, P. Xie, Z. Wang, Y. Qu, Z. Zhang, Y. Liu, R. Fan, Tailorable radio-frequency negative permittivity of titanium nitride sintered with different oxidation pretreatments. *Ceram. Int.* **43**, 16980–16985 (2017)
- P. Xie, W. Sun, Y. Liu, A. Du, Z. Zhang, G. Wu, R. Fan, Carbon aerogels towards new candidates for double negative metamaterials of low density. *Carbon* **129**, 598–606 (2017)
- K. Sun, P. Xie, Z. Wang, T. Su, Q. Shao, J. Ryu, X. Zhang, J. Guo, A. Shankar, J. Li, Flexible polydimethylsiloxane/multi-walled carbon nanotubes membranous metamaterials with negative permittivity. *Polymer* **125**, 50–57 (2017)
- P. Xie, K. Sun, Z. Wang, Y. Liu, R. Fan, Z. Zhang, G. Schumacher, Negative permittivity adjusted by SiO<sub>2</sub>-coated metallic particles in percolative composites. *J. Alloys Compd.* **725**, 1259–1263 (2017)
- P. Xie, Z. Wang, K. Sun, C. Cheng, Y. Liu, R. Fan, Regulation mechanism of negative permittivity in percolating composites via building blocks. *Appl. Phys. Lett.* **111**, 112903 (2017)
- Z.C. Shi, R.H. Fan, K.L. Yan, K. Sun, M. Zhang, C.G. Wang, X.F. Liu, X.H. Zhang, Preparation of iron networks hosted in porous alumina with tunable negative permittivity and permeability. *Adv. Func. Mater.* **23**, 4123–4132 (2013)
- Z.C. Shi, R.H. Fan, Z.D. Zhang, H.Y. Gong, J. Ouyang, Y.J. Bai, X.H. Zhang, L.W. Yin, Experimental/theoretical investigation on the high frequency dielectric properties of Ag/Al<sub>2</sub>O<sub>3</sub> composites. *Appl. Phys. Lett.* **99**, 137401 (2011)
- Z. Shi, S. Chen, K. Sun, X. Wang, R.-H. Fan, X.-A. Wang, Tunable radio-frequency negative permittivity in nickel-alumina “natural” meta-composites. *Appl. Phys. Lett.* **104**, 52–3398 (2014)
- X.A. Wang, Z.C. Shi, M. Chen, R.H. Fan, K.L. Yan, K. Sun, S.B. Pan, M.X. Yu, Tunable electromagnetic properties in Co/Al<sub>2</sub>O<sub>3</sub> cermets prepared by wet chemical method. *J. Am. Ceram. Soc.* **97**, 3223–3229 (2014)
- Z. Shi, F. Mao, J. Wang, R. Fan, X. Wang, Percolative silver/alumina composites with radio frequency dielectric resonance-induced negative permittivity. *RSC Adv.* **5**, 107307–107312 (2015)
- Y. Qu, P. Xie, G. Fan, Y. Liu, Y. Wu, L. Zhang, R. Fan, Strategy of adjusting negative permittivity with invariant permeability property in metallic granular percolating composites. *J. Mater. Sci. Mater. Electron.* (2017). <https://doi.org/10.1007/s10854-017-8027-7>
- M. Han, X. Yin, X. Li, B. Anasori, L. Zhang, L. Cheng, Y. Gogotsi, Laminated and two-dimensional carbon-supported microwave absorbers derived from MXenes. *ACS Appl. Mater. Interfaces* **9**, 20038–20045 (2017)
- M. Han, X. Yin, Z. Hou, C. Song, X. Li, L. Zhang, L. Cheng, Flexible and thermostable graphene/SiC nanowires foam composites with tunable electromagnetic wave absorption properties. *ACS Appl. Mater. Interfaces* **9**, 11803–11810 (2017)
- M. Han, X. Yin, W. Duan, S. Ren, L. Zhang, L. Cheng, Hierarchical graphene/SiC nanowire networks in polymer-derived ceramics with enhanced electromagnetic wave absorbing capability. *J. Eur. Ceram. Soc.* **36**, 2695–2703 (2016)
- M. Han, X. Yin, S. Ren, W. Duan, L. Zhang, L. Cheng, Core/shell structured C/ZnO nanoparticles composites for effective electromagnetic wave absorption. *RSC Adv.* **6**, 6467–6474 (2016)
- W. Li, U. Guler, N. Kinsey, G.V. Naik, A. Boltasseva, J. Guan, V.M. Shalaev, A.V. Kildishev, Refractory plasmonics with titanium nitride: broadband metamaterial absorber. *Adv. Mater.* **26**, 7959–7965 (2014)
- X. Hou, P. Qiu, T. Yang, K.-C. Chou, Synthesis of titanium nitride nanopowder at low temperature from the combustion synthesized precursor and the thermal stability. *J. Alloys Compd.* **615**, 838–842 (2014)
- M. Cortie, J. Giddings, A. Dowd, Optical properties and plasmon resonances of titanium nitride nanostructures. *Nanotechnology* **21**, 115201 (2010)
- X. Wu, Q. Wang, W. Zhang, Y. Wang, W. Chen, Nano nickel oxide coated graphene/polyaniline composite film with high electrochemical performance for flexible supercapacitor. *Electrochim. Acta* **211**, 1066–1075 (2016)
- Z.B. Wen, F. Yu, T. You, L. Zhu, L. Zhang, Y.P. Wu, A core–shell structured nanocomposite of NiO with carbon nanotubes as positive electrode material of high capacitance for supercapacitors. *Mater. Res. Bull.* **74**, 241–247 (2016)



33. H. Haruta, The impedance measurement handbook: a guide to measurement technology and techniques. Agilent Technologies (2000)
34. C. Cheng, K. Yan, R. Fan, L. Qian, Z. Zhang, K. Sun, M. Chen, Negative permittivity behavior in the carbon/silicon nitride composites prepared by impregnation-carbonization approach. *Carbon* **96**, 678–684 (2016)
35. K. Yan, R. Fan, Z. Shi, M. Chen, L. Qian, Y. Wei, K. Sun, J. Li, Negative permittivity behavior and magnetic performance of perovskite  $\text{La}_{1-x}\text{Sr}_x\text{MnO}_3$  at high-frequency. *J. Mater. Chem. C* **2**, 1028–1033 (2014)
36. H. Wu, R. Yin, L. Qian, Z. Zhang, Three-dimensional graphene network/phenolic resin composites towards tunable and weakly negative permittivity. *Mater. Design* **117**, 18–23 (2017)
37. F. He, S. Lau, H.L. Chan, J. Fan, High dielectric permittivity and low percolation threshold in nanocomposites based on poly(vinylidene fluoride) and exfoliated graphite nanoplates. *Adv. Mater.* **21**, 710–715 (2010)
38. J. Wang, Z.C. Shi, F. Mao, S. Chen, X. Wang, Bilayer polymer metacomposites containing negative permittivity layer for new high-k materials. *ACS Appl. Mater. Interfaces* **9**, 1793–1800 (2016)
39. H. Gu, H. Zhang, C. Ma, S. Lyu, F. Yao, C. Liang, X. Yang, J. Guo, Z. Guo, J. Gu, Polyaniline assisted uniform dispersion for magnetic ultrafine barium ferrite nanorods reinforced epoxy metacomposites with tailorable negative permittivity. *J. Phys. Chem. C* **121**, 13265–13273 (2017)
40. X. Zhang, X. Yan, Q. He, H. Wei, J. Long, J. Guo, H. Gu, J. Yu, J. Liu, D. Ding, Electrically conductive polypropylene nanocomposites with negative permittivity at low carbon nanotube loading levels. *ACS Appl. Mater. Interfaces* **7**, 6125–6138 (2015)
41. Y. Feng, W. Li, Y. Hou, Y. Yu, W. Cao, T. Zhang, W. Fei, Enhanced dielectric properties of PVDF-HFP/BaTiO<sub>3</sub>-nanowire composites induced by interfacial polarization and wire-shape. *J. Mater. Chem. C* **3**, 1250–1260 (2015)
42. C. Wu, X. Huang, X. Wu, L. Xie, K. Yang, P. Jiang, Graphene oxide-encapsulated carbon nanotube hybrids for high dielectric performance nanocomposites with enhanced energy storage density. *Nanoscale* **5**, 3847–3855 (2013)
43. Z. Wang, K. Sun, P. Xie, Y. Liu, R. Fan, Generation mechanism of negative permittivity and Kramers–Kronig relations in BaTiO<sub>3</sub>/Y<sub>3</sub>Fe<sub>5</sub>O<sub>12</sub> multiferroic composites. *J. Phys.: Condens. Matter* **29**, 365703 (2017)
44. J. Zhang, M. Mine, D. Zhu, M. Matsuo, Electrical and dielectric behaviors and their origins in the three-dimensional polyvinyl alcohol/MWCNT composites with low percolation threshold. *Carbon* **47**, 1311–1320 (2009)
45. G. Liu, P. Ci, S. Dong, Energy harvesting from ambient low-frequency magnetic field using magneto-mechano-electric composite cantilever. *Appl. Phys. Lett.* **104**, 032908 (2014)
46. M. Han, X. Yin, L. Kong, M. Li, W. Duan, L. Zhang, L. Cheng, Graphene-wrapped ZnO hollow spheres with enhanced electromagnetic wave absorption properties. *J. Mater. Chem. A* **2**, 16403–16409 (2014)